RSC Advances

ROYAL SOCIETY OF CHEMISTRY

www.rsc.org/advances

Graphical Abstract

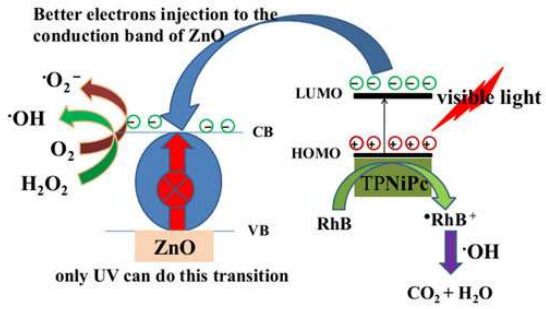

ZnO–NRs/TPNiPc hierarchical hetero-nanostructure arrays exhibited superior visible light photocatalytic activities in degradation of Rhodamine B assisted with H_2O_2.

ZnO nanorods/ nickel phthalocyanine hierarchical hetero-nanostructures with superior visible light photocatalytic propertities assisted with H_2O_2

Xiuhua Wang[ab]*, Jie Gao[a], Bingang Xu[b]*, Tao Hua[b], Houyong Xia[a]

[a]The Key Laboratory of Functional Molecular Solids, Ministry of Education, College of Chemistry and Materials Science, Anhui Normal University, Wuhu 241000, China

[b]Nanotechnology Center, Institute of Textiles and Clothing, The Hong Kong Polytechnic University, Hung Hom, Kowloon, Hong Kong, P. R. China

* To whom correspondence should be addressed:

E-mail: xhwang@mail.ahnu.edu.cn, tcxubg@polyu.edu.hk

Abstract

Needle-like ZnO nanorods (ZnO–NRs)/2,9,16,23-tetra-phenoxy nickel phthalocyanine (TPNiPc) nanofibers hierarchical hetero-nanostructures have been successfully designed and constructed via a two-step hydrothermal approach on zinc foil. The as-prepared ZnO–NRs/TPNiPc hierarchical hetero-nanostructure exhibited superior photocatalytic activities in degradation of Rhodamine B assisted with H_2O_2 under visible light irradiation with excellent efficiency, recyclability and stability. The intermolecular electron transfer in the process of photocatalytic was further confirmed by the enhanced photocurrent. This method offers a simple, economical, and convenient way to obtain high efficient visible-light photocatalyst based on ZnO, showing great industrial application potential in eliminating the organic pollutants from wastewater.

Keywords: ZnO nanorods; nickel phthalocyanine; hierarchical hetero-nanostructure; photocatalytic

1. Introduction

With fast development of industrialization, environment pollution has attracted intensive global concern. Among the various pollutants, the pollution of water resources by dyes from the textile has become a serious environmental problem. In order to remove the dyes from the aqueous environment, various methods have been explored, such as photocatalysis, adsorption, electrochemical degradation, acidification, etc.[1] Among the above-mentioned methods, photocatalysis technology has been applied extensively to remove organic pollutants from aqueous solutions owing to its simplicity, speed, low cost, high removal capacity, low secondary pollution and environmentally friendly nature.[2-4]

As an important wide and direct band-gap semiconductor, ZnO has been deemed to be an efficient photocatalyst because of its high catalytic efficiency, low cost, and environmental sustainability.[5-7] However, a major handicap is its rather large optical band gap (3.2 eV), which means it can only be activated by ultraviolet (UV) light ($\lambda <$ 400 nm). According to the solar spectrum, UV light accounts for only a small fraction (4–6%) of the incoming solar energy, whereas visible light makes up as large as 43%. For the more efficient utilization of the incoming light energy, considerable research efforts have been directed toward exploring visible-light photocatalysts.[8-10] The rapid recombination of photogenerated electron–hole pairs formed in photocatalytic processes is also a major obstacle for increasing the photocatalytic efficiency of ZnO. In order to overcome these drawbacks, efforts have been made via combination ZnO with other components including inorganic or organic semiconductor, noble metals, and grapheme et al.[11-14]

Owing to the appropriate redox properties for the sensitization of large band-gap semiconductors and the thermal stability, metal phthalocyanine (MPc) have received significant attention for advanced applications in dye-sensitized solar cells, gas sensors and molecular electronic devices.[15-20] More recently, it has been demonstrated that MPc could hinder the charge recombination and improve the photocatalytic efficiency.[21-26] For example, Oki et.al prepared ZnO and cobalt phthalocyanine hybridized graphene as photocatalyst of degradation of rhodamine B (RhB) for about

140 min under exposure to natural sunlight.[23] Nyokong et.al reported the photocatalytic transformation of Rhodamine 6G using tetracarbazole zinc phthalocyanine conjugated with ZnO macroparticles and silver nanoparticles and 65% of Rhodamine 6G had been degraded within 60 min at pH 9.[24] Yang and Lu groups successfully synthesized manganese phthalocyanine covalently functionalized graphene nanohybrid via 1,3-dipolar cycloaddition for a photocatalyst and the results showed that intermolecular electron transfer was facilitated and the photoexcited charges recombination was suppressed as confirmed by the fluorescence quenching and enhanced photocurrent density.[27]

Though valuable work has been carried out towards degradation efficiency, there are still potential challenges to be considered. For instance, doped too much materials may suffer from photocorrosion, thermal instability, lattice distortion, and an increase in recontamination and the carrier-recombination probability. Thus, we need one effective reagent, which can effectively modify the surface of ZnO and leave no pollution in the environment. To our knowledge, there has been no report on the degradation of RhB dye by ZnO/MPc hierarchical hetero-nanostructure arrays assisted with H_2O_2 under visible light.

In this paper, we report a successful attempt at the fabrication of 2,9,16,23-tetra-phenoxy nickel phthalocyanine (TPNiPc) nanostructure grown on the ZnO nanorods (ZnO–NRs) based on zinc substrate by a facile two-step of hydrothermal method. TPNiPc can be fixed onto ZnO–NRs, which could avoid phthalocyanines enter into the environment to cause additional pollution. The as-obtained ZnO–NRs/TPNiPc hierarchical hetero-nanostructure arrays had high photocatalytic activity, recyclability and stability toward the decomposition of RhB in the presence of H_2O_2 under visible light irradiation. It is expected that the ZnO–NRs/TPNiPc hierarchical hetero-nanostructure with high visible light photocatalytic activity will greatly promote their industrial applications in organic wastewater treatment.

2. Experimental section

2.1 Reagents

4-Phenoxyphthalonitrile, nickel(II) chloride hexahydrate ($NiCl_2 \cdot 6H_2O$), ammonium molybdate ($(NH_4)_2Mo_2O_7$), zinc foil, glycol, ethylenediamine and ethanol were purchased from Sinopharm Chemical Reagent Co., Ltd. All these reagents were of analytical grade and used without further purification. Deionized water was used throughout.

2.2 Synthesis of ZnO–NRs on the zinc substrate

The synthesis of a ZnO nanorods (ZnO–NRs) array was performed on zinc foil. In the synthesis, the commercial zinc foil (99.9%, 2×3 cm) was washed with ethanol and diluted hydrochloric acid respectively in an ultrasonic pool. 5 mL of ethylenediamine was dissolved in 30 mL of distilled water in a 50 mL Teflon-lined stainless steel autoclave. Then the zinc foil was inclined and inserted into the solution. The autoclave was sealed and maintained at 160 ^oC for 5 h, then allowed to cool to room temperature naturally. The white precipitate covered on both sides of the zinc foil was washed with distilled water and ethanol several times, then dried in a vacuum at 50 ^oC overnight.

2.3 Synthesis of ZnO–NRs /TPNiPc hierarchical hetero-nanostructure

10 mL ethylene glycol was added into 10 mL distilled water under the magnetic string, and then 0.05 g of 4-Phenoxyphthalonitrile, 0.01 g of $NiCl_2 \cdot 6H_2O$ and 5 mg of ammonium molybdate were dissolved in the mixed solution. After stirring for 10 min, the solution was loaded into a 50 mL Teflon-lined stainless steel autoclave with the zinc foil covered by white precipitate inserted. The autoclave was sealed and maintained in an electric oven at 180 ^oC for 12 h. After the autoclave was cooled down to room temperature naturally, the black precipitates covered on the zinc foil were collected, washed with distilled water and ethanol for several times, and then dried at 50 ^oC overnight.

2.4 Material characterization

X-ray powder diffraction (XRD) patterns have been recorded on a Rigaku Max-2200 with Cu Kα radiation. The scanning electron microscopy (SEM) images

have been taken with a Hitachi S-4800 field-emission scanning electron microscope. UV-visible diffuse reflectance spectra were recorded on a Hitachi U-2050 spectrophotometer using magnesium oxide as a standard. The Fourier transform infrared (FTIR) spectroscopic study was carried out with a Shimadzu FTIR-8400S spectrometer.

2.5 Photocatalytic experiments

Photocatalytic activities of the synthesized ZnO–NRs/TPNiPc hierarchical hetero-nanostructure arrays were evaluated with RhB as a representative dye pollutant under Xe Lamp irradiation. The precipitates covered zinc foil was cut into 1 × 1.5 cm and placed in the bottom of a beaker (150 mL) containing 50 mL of 0.01g/L RhB aqueous solution and 0.5 mL H_2O_2 and placed in the dark for 1 h to reach the adsorption/desorption equilibrium on the catalyst surface. Then, visible light irradiation was carried out with a 300 W Xe lamp. A 600 nm glass cut-off filter (Schott) was used to filter off ultraviolet radiations. At a given time interval of 20 minutes, the absorbance spectra of the solution were recorded using a UV-vis spectrophotometer (Shimadzu UV-2550), from which the concentration of RhB was measured by monitoring its characteristic absorption at 552 nm.

2.6 Photocurrent measurements

The photoconductivity measurements were tracked with a CHI 660D (CHI Instruments, Chenhua Corp., Shanghai, China) electrochemical workstation. The precipitates covered on zinc foil (1 × 1.5 cm) were directly as the electrode. Light was supplied by a 300 W Xe lamp with filter off ultraviolet radiations.

3. Results and discussion

3.1. Material characterization

The crystal structure and phase composition of ZnO–NRs/TPNiPc hierarchical hetero-nanostructures, ZnO–NRs and TPNiPc microspheres were revealed by XRD analysis. The curve (a) in Fig. 1 demonstrates that the ZnO–NRs are well-crystallized and all of the diffraction peaks can be perfectly indexed to hexagonal phase ZnO (JCPDS No. 79-0206) and no excrescent peaks are detectable, indicating the high purity of the product. The curve (b) in Fig. 1 is the XRD pattern of the TPNiPc

obtained directly without the zinc foil. After the second hydrothermal treatment, as shown in curve (c), additional diffraction peaks with 2θ values of 27° and 42° appeared, corresponding to the XRD pattern of the TPNiPc, indicating that the as-synthesized sample is composed of ZnO and TPNiPc phases on the zinc substrate.

The FTIR spectrum is recorded to reveal the composition and the phase of products as shown in Figure 2. The aromatic amine resonances (C–N, 1580 cm^{-1}) and aromatic stretching (C=C, 1483 cm^{-1}) are clearly observed. The peaks at 1240 and 1086 cm^{-1} are attributed to the asymmetric and symmetric stretching vibrations of ether bond (C–O–C). The peaks at 687, 757 cm^{-1} might be assigned to phthalocyanine skeletal vibration. The peak at 833 cm^{-1} is assigned to the Ni–N stretching vibration.[23] The IR active characteristic peak of ZnO is observed in the spectral range 400–600 cm^{-1}.[28] These peaks were also observed in the FT-IR spectra of pure TPNiPc and ZnO–NRs. The above results revealed that TPNiPc was successfully coated onto the surface of ZnO–NRs.

The morphology and size of the samples were observed by the FESEM. After the first hydrothermal treatment, it can be clearly seen that the needle-like ZnO nanorods with average 610 nm wide and twenty micrometers long could be obtained, as shown in Figs. 3a and b. After the second hydrothermal treatment, the product displays hierarchical hetero-nanostructure as shown in Figs. 3c and d, where secondary TPNiPc microplates consisted with average diameter of 100 nm nanofibers are assembled and aggregated on the top of nanorods. The more detailed structural characteristics of the TPNiPc microplates can be revealed from the SEM image with high magnification (Fig. 3d).

3.2 The growth mechanism

In order to explore the formation mechanism of ZnO–NRs/TPNiPc hierarchical hetero-nanostructures, a series of various conditional experiments were carried out and the intermediate products were characterized by SEM. When the heating temperature is 200 °C, large TPNiPc particles with an average diameter of 900 nm are assembled on the primary ZnO–NRs, as shown in Figs. 4a and b. If the heating temperature was under 120 °C, few ZnO–NRs/TPNiPc hierarchical

hetero-nanostructure was formed. When we changed the dosage of 4-Phenoxyphthalonitrile to 0.025 g (other reactants without changed), we could obtain a few ZnO–NRs/TPNiPc hierarchical hetero-nanostructures, as shown in Figs. 4c and d.

There are also several other factors that affect the morphology and uniformity of ZnO–NRs/TPNiPc hierarchical hetero-nanostructures, such as heating time. If the heating time is below 12h, only a few ZnO–NRs/TPNiPc hierarchical hetero-nanostructures were obtained, as shown in Figs. 4e and f. From a series of experiments, temperature of 180 ^{o}C, the dosage of 0.05 g 4-Phenoxyphthalonitrile and a hydrothermal time of 12 h are found to the optimum conditions to obtain high quality ZnO–NRs/TPNiPc hierarchical hetero-nanostructure. The morphology of TPNiPc obtained directly without the zinc foil (other conditions without changed, Fig. S1) is smooth microplates, which indicates that there may be tip growth model for the TPNiPc nanostructure grown onto ZnO–NRs. Based on the experimental results, we propose that the growth mechanism could be ascribed to a solid-solution-solid transformation and tip growth model. The formation mechanism of ZnO–NRs/TPNiPc hierarchical hetero-nanostructures is schematically shown in Scheme 1.

3.3 Photocatalytic activities

The photocatalytic degradation of RhB had been chosen as a model reaction to evaluate the photocatalytic activities of the ZnO–NRs/TPNiPc hierarchical hetero-nanostructure arrays assisted with or without H_2O_2, pure TPNiPc and ZnO–NRs assisted with H_2O_2 and pure H_2O_2 under visible light irradiation (Fig. 5 and Fig. S2). Fig. 5a shows the absorption spectra of an aqueous solution of RhB with ZnO–NRs/TPNiPc hierarchical hetero-nanostructures assisted with H_2O_2 exposed to visible light irradiation for various time periods. The absorption peak at λ = 552 nm diminishes gradually as the irradiation time increases, and completely disappears after about 2 h. No new absorption peak appears in either the visible or ultraviolet regions, which indicates the complete photocatalytic degradation of RhB during the reaction.

Fig. 5 b shows the variation of the concentrations of RhB solution in the presence of ZnO–NRs/TPNiPc hierarchical hetero-nanostructure arrays assisted with or without

H_2O_2, TPNiPc assisted with H_2O_2, ZnO–NRs assisted with H_2O_2 and pure H_2O_2 under visible light irradiation. It is obvious that ZnO–NRs/TPNiPc hierarchical hetero-nanostructure arrays exhibit superior photocatalytic abilities compared with other photocatalysts. The enhanced photocatalytic performance of ZnO–NRs/TPNiPc hierarchical hetero-nanostructure arrays was benefited from the cooperative role of the two components of the photocatalyst assisted with H_2O_2, TPNiPc promoting the light absorption in the visible range and ZnO–NRs acting as an acceptor of electrons generated by the photons absorption to produce superoxide radicals.

The photocatalytic stability of ZnO–NRs/TPNiPc hierarchical hetero-nanostructure catalyst is also carried out by repetitively testing the sample in the fresh RhB solution under the visible light irradiation for three cycles (Fig. 6). The efficiency for the degradation of RhB has little change even after the third cycle, exhibiting a good durability.

The UV-vis diffuse reflectance spectra were investigated to reveal the light absorbance performances of ZnO–NRs/TPNiPc hierarchical hetero-nanostructure arrays, TPNiPc and ZnO–NRs, as shown in Fig. 7a. There is a new broad absorbance in the visible light region for ZnO–NRs/TPNiPc hierarchical hetero-nanostructure arrays sample, implying that the coupling structure of ZnO–NRs nanostructure with TPNiPc may have efficient visible-light sensitive photocatalysis. By calculation from the UV diffuse reflection spectra with the Tauc equation ($\alpha h\nu = A\ (h\nu - E_g)^{n/2}$),[29, 30] the optical band gaps of ZnO–NRs/TPNiPc is 2.15 eV, which is smaller than the pure ZnO–NRs (3.2 eV), as shown in Fig. 7b. The red shift of the band gap demonstrated the higher photocatalytic activities of ZnO–NRs/TPNiPc hierarchical hetero-nanostructure arrays under visible-light irradiation.

3.4 Photocurrent performance

To further study the enrichment of the photocatalytic activity, photocurrent measurements were performed for investigating the electron transfer between the ZnO–NRs moiety and TPNiPc under visible light irradiation. Fig. 8a shows the *I–V* curves measured in dark and under illumination by using a 300 W Xe lamp (with power of 15A). Both of them exhibit good linear behavior, which proves a fine ohmic

contact. However, the photocurrent of ZnO–NRs/TPNiPc hierarchical hetero-nanostructure arrays under illumination increases largely as compared to that in dark, as shown in Fig. 8a. The significant improvement of photocurrent response of the ZnO–NRs/TPNiPc hierarchical hetero-nanostructure arrays electrode may be attributed to the nice absorption of TPNiPc in the visible-light range and efficient electron transfer from the photoexcited TPNiPc moiety to the covalently bonded ZnO–NRs.[31, 32] All the photocurrent results indicate that photocatalytic process is essentially a process of electron transfer.[33, 34]

We also investigated the photocurrent response of ZnO–NRs/TPNiPc hierarchical hetero-nanostructure arrays electrode under the different power, as shown in Fig. 8b. It is obvious that the power of the irradiation light has no big influence on the photocurrent of ZnO–NRs/TPNiPc hierarchical hetero-nanostructure arrays electrode, which indicates that the ZnO–NRs/TPNiPc hierarchical hetero-nanostructure is robust with less consideration of the application condition.

The effects of H_2O_2 on the I–V curves of ZnO–NRs/TPNiPc hierarchical hetero-nanostructures in dark and under illumination by using a 300 W Xe lamp (15A) were further performed, as shown in Fig. 9. It is obvious that the photocurrent response of the ZnO–NRs/TPNiPc electrode assisted with H_2O_2 has significant improvement, which may be attributed to that H_2O_2 facilitates the generation of hydroxyl radicals and promotes the photodecolorization effectively. And, it could also inhibit the recombination of electron−hole pairs. [35-38]

Based on the above results and the earlier reports on the dye-sensitized photocatalytic oxidation of pollutants, [21, 24] a proposed photocatalytic mechanism of H_2O_2 assisted photocatalytic degradation of RhB in visible light irradiation with the ZnO–NRs/TPNiPc hierarchical hetero-nanostructure was presumed, as shown in Scheme 2. And the mechanism for the photocatalytic degradation of RhB in our experiment was proposed as follows:

$$TPNiPc + hv \rightarrow TPNiPc^* \quad (1)$$

$$TPNiPc^* + O_2 \rightarrow TPNiPc + {}^1O_2 \quad (2)$$

$$NiPc^* + ZnO \rightarrow {}^{\bullet}TPNiPc^{+} + ZnO\ (e^{-}) \quad (3)$$

$^{\bullet}TPNiPc^{+} + RTPhB \rightarrow TPNiPc + {}^{\bullet}RhB^{+}$ (4)

$ZnO\ (e^{-}) + O_2 \text{ or } {}^{1}O_2 \rightarrow ZnO + {}^{\bullet}O_2^{-}$ (5)

$ZnO\ (e^{-}) + H_2O_2 \rightarrow OH^{-} + {}^{\bullet}OH$ (6)

$^{\bullet}O_2^{-} + H_2O \rightarrow {}^{\bullet}HO_2 + OH^{-}$ (7)

$^{\bullet}HO_2 + H_2O \rightarrow H_2O_2 + {}^{\bullet}OH$ (8)

$H_2O_2 \rightarrow 2{}^{\bullet}OH$ (9)

$RhB + {}^{\bullet}OH \rightarrow CO_2 + H_2O$ (10)

The MPc in the solid state behave as p-type semiconductors, characterized by energy of the band gap about 2.0 eV. [39] Upon irradiation with light $\lambda > 400$ nm, it was possible to excite only the TPNiPc particles supported on nanorods and generated the singlet oxygen ($^{1}O_2$) via energy transfer (Eqs. 1 and 2).[5, 24] The excited charge was then injected from the excited state of TPNiPc into the conduction band of ZnO, followed by generation of the TPNiPc cation radical ($^{\bullet}TPNiPc^{+}$) and conduction band electrons (e_{cb}^{-}) of ZnO (Eq. 3). The $^{\bullet}TPNiPc^{+}$ could oxidize RhB, together with recovery of the original TPNiPc (Eq. 4).[40] O_2 and $^{1}O_2$ reacted with conduction band electrons (e_{cb}^{-}) to yield superoxide radical anions ($^{\bullet}O_2^{-}$), which protonation generated the hydroperoxy radicals ($^{\bullet}HO_2$), subsequently producing hydroxyl radicals ($^{\bullet}OH$) (Eqs. 5-9).[40, 41] In this case, the RhB molecules can be destroyed into CO_2 and H_2O by the generated $^{\bullet}OH$ radicals owing to their high activities (Eq. 10). At the same time, H_2O_2, used as efficient electron scavenger, can react with excited electrons of semiconductors to form more $^{\bullet}OH$ radicals and enhance the photocatalytic ability largely. Because of the high absorption capacity and the increased amount of excited electrons, RhB molecules absorbed on the surface of ZnO–NRs/TPNiPc hierarchical hetero-nanostructure arrays could be easily photodegradated.

4. Conclusion

In summary, ZnO–NRs/TPNiPc hierarchical hetero-nanostructure arrays were successfully synthesized via two-step of hydrothermal conditions without any template and surfactant. The growth mechanism could be ascribed to a solid-solution-solid transformation mechanism. The as-prepared ZnO–NRs/TPNiPc

hierarchical hetero-nanostructure exhibited superior photocatalytic activities in degradation of RhB under visible light irradiation, which may be attributed to the cooperative role of the two components of the photocatalyst assisted with H_2O_2. Furthermore, the largely increased photocurrent response sensitivity of the ZnO–NRs/TPNiPc hierarchical hetero-nanostructure under visible light irradiation demonstrated that the electron transfer in the process of photocatalysis. The facile method developed here can also be extended to construction of other high visible light photocatalyst based on ZnO.

Acknowledgements

The financial support from the Natural Science Foundation of China (No. 21301007) and the Hong Kong Polytechnic University (No. G-YM57) are acknowledged.

References

1. A. Kudo and Y. Miseki, *Chem. Soc. Rev.*, 2009, 38, 253-278.
2. A. R. Amani-Ghadim and M. S. S. Dorraji, *Appl. Catal. B Env.*, 2015, 163, 539-546.
3. H. Li, Y. Zhou, W. Tu, J. Ye and Z. Zou, *Adv. Funct. Mater.*, 2015, 25, 998-1013.
4. H. Huang, X. Han, X. Li, S. Wang, P. K. Chu and Y. Zhang, *ACS Appl. Mater. Interfaces*, 2015, 7, 482-492.
5. H.-L. Guo, Q. Zhu, X.-L. Wu, Y.-F. Jiang, X. Xie and A.-W. Xu, *Nanoscale*, 2015, 7, 7216-7223.
6. V. Roge, N. Bahlawane, G. Lamblin, I. Fechete, F. Garin, A. Dinia and D. Lenoble, *J. Mater. Chem. A*, 2015, 3, 11453-11461.
7. Y. Liu, L. Yu, Y. Hu, C. F. Guo, F. M. Zhang and X. W. Lou, *Nanoscale*, 2012, 4, 183-187.
8. A. Yarahmadi and S. Sharifnia, *Dyes Pigm.*, 2014, 107, 140-145.
9. S. Ren, B. Wang, H. Zhang, P. Ding and Q. Wang, *ACS Appl. Mater. Interfaces*, 2015, 7, 4066-4074.
10. R. Lamba, A. Umar, S. K. Mehta and S. K. Kansal, *Talanta*, 2015, 131, 490-498.

11. Y. Jin, J. Xi, Z. Zhang, J. Xiao, F. Xiao, L. Qian and S. Wang, *Nanoscale*, 2015, 7, 5510-5515.
12. S. Adhikari, D. Sarkar and G. Madras, *Rsc Adv.*, 2015, 5, 11895-11904.
13. Y. Chen, D. Zeng, M. B. Cortie, A. Dowd, H. Guo, J. Wang and D.-L. Peng, *Small*, 2015, 11, 1460-1469.
14. K. Mohanta, S. K. Batabyal and A. J. Pal, *Adv. Funct. Mater.*, 2008, 18, 687-693.
15. J. Huang, Y. Wu, D. Wang, Y. Ma, Z. Yue, Y. Lu, M. Zhang, Z. Zhang and P. Yang, *ACS Appl. Mater. Interfaces*, 2015, 7, 3732-3741.
16. A. Hamdi, S. Boufi and S. Bouattour, *Appl. Surf. Sci.*, 2015, 339, 128-136.
17. W. Riedel, S. Wiesner, D. Greiner, V. Hinrichs, M. Rusu and M. C. Lux-Steiner, *Appl. Phys. Lett.*, 2014, 104.
18. B. H. Lessard, R. T. White, M. Al-Amar, T. Plint, J. S. Castrucci, D. S. Josey, Z.-H. Lu and T. P. Bender, *ACS Appl. Mater. Interfaces*, 2015, 7, 5076-5088.
19. X. Zhang, L. Yu, C. Zhuang, T. Peng, R. Li and X. Li, *Rsc Adv.*, 2013, 3, 14363-14370.
20. R. Narayanan, M. Deepa and A. K. Srivastava, *J. Mater. Chem. A*, 2013, 1, 3907-3918.
21. Z. Guo, B. Chen, J. Mu, M. Zhang, P. Zhang, Z. Zhang, J. Wang, X. Zhang, Y. Sun, C. Shao and Y. Liu, *J. Hazard. Mater.*, 2012, 219, 156-163.
22. M. Zhang, C. Shao, Z. Guo, Z. Zhang, J. Mu, T. Cao and Y. Liu, *ACS Appl. Mater. Interfaces*, 2011, 3, 369-377.
23. G. M. Neelgund, A. Oki and Z. Luo, *J. Colloid Interface Sci.*, 2014, 430, 257-264.
24. P. Khoza and T. Nyokong, *J. Coord. Chem.*, 2015, 68, 1117-1131.
25. M. Zhang, C. Shao, Z. Guo, Z. Zhang, J. Mu, P. Zhang, T. Cao and Y. Liu, *ACS Appl. Mater. Interfaces*, 2011, 3, 2573-2578.
26. A. Chunder, T. Pal, S. I. Khondaker and L. Zhai, *J. Phys. Chem. C*, 2010, 114, 15129-15135.

27. D. D. Wang, J. Huang, X. Li, P. Yang, Y. K. Du, C. M. Goh and C. Lu, *J. Mater. Chem. A*, 2015, 3, 4195-4202.

28. M. Ghosh, N. Padma, R. Tewari and A. K. Debnath, *J. Phys. Chem. C*, 2014, 118, 691-699.

29. S. J. Hong, S. Lee, J. S. Jang and J. S. Lee, *Energy Environ. Sci.*, 2011, 4, 1781-1787.

30. H. F. Cheng, B. B. Huang, X. Y. Qin, X. Y. Zhang and Y. Dai, *Chem. Commun.*, 2012, 48, 97-99.

31. L. Heng, D. Tian, L. Chen, J. Su, J. Zhai, D. Han and L. Jiang, *Chem. Commun.*, 2010, 46, 1162-1164.

32. Q. Chen, H. Ding, Y. Wu, M. Sui, W. Lu, B. Wang, W. Su, Z. Cui and L. Chen, *Nanoscale*, 2013, 5, 4162-4165.

33. Y. Chen, H. Zhao, B. Liu and H. Yang, *Appl. Catal. B Env.*, 2015, 163, 189-197.

34. S. Mubeen, J. Lee, N. Singh, S. Kraemer, G. D. Stucky and M. Moskovits, *Nat. Nanotechnol.*, 2013, 8, 247-251.

35. F. Chen, P. Fang, Y. Gao, Z. Liu, Y. Liu and Y. Dai, *Chem. Eng. J.*, 2012, 204, 107-113.

36. S. Navalon, D. Sempere, M. Alvaro and H. Garcia, *ACS Appl. Mater. Interfaces*, 2013, 5, 7160-7169.

37. X. An, X. Yu, J. C. Yu and G. Zhang, *J. Mater. Chem. A*, 2013, 1, 5158-5164.

38. L. H. Han, Y. C. Chen and Y. Wei, *CrystEngComm*, 2012, 14, 4692-4698.

39. C.-Y. Zhong, H.-B. Pan, N.-S. Chen, J.-L. Huang and L.-F. Guo, *Chinese Journal of Inorganic Chemistry*, 2007, 23, 1901-1906.

40. R. R. Salinas-Guzman, J. L. Guzman-Mar, L. Hinojosa-Reyes, J. M. Peralta-Hernandez and A. Hernandez-Ramirez, *J. Sol-Gel Sci. Technol.*, 2010, 54, 1-7.

41. P. Khoza and T. Nyokong, *Journal of Molecular Catalysis a-Chemical*, 2015, 399, 25-32.

Figures captions

Figure 1. XRD patterns of ZnO–NRs/TPNiPc hierarchical hetero-nanostructures, TPNiPc and ZnO–NRs.

Figure 2. FTIR spectra of ZnO–NRs/TPNiPc hierarchical hetero-nanostructures, TPNiPc and ZnO–NRs.

Figure 3. (a, b) FESEM images of ZnO–NRs; (c, d) FESEM images of the ZnO–NRs/TPNiPc hierarchical hetero-nanostructures.

Figure 4. FESEM images of the ZnO–NRs/TPNiPc hierarchical hetero-structures attained at different reaction conditions: (a, b) at 200 ^{o}C; (c, d) the dosage of 4-Phenoxyphthalonitrile is 0.025 g; (e) the heating time is under 5 h; (f) the heating time is about 10 h.

Figure 5. (a) Absorption spectra of the RhB solution by ZnO–NRs/TPNiPc hierarchical hetero-nanostructures assisted with H_2O_2 under visible light irradiation; (b) RhB photodegradation curves of C/C_0 versus time by ZnO–NRs/TPNiPc hierarchical hetero-nanostructures assisted with or without H_2O_2, TPNiPc assisted with H_2O_2, ZnO–NRs assisted with H_2O_2 and pure H_2O_2 under visible light irradiation, where C_0 and C are the initial concentration and the reaction concentration of RhB, respectively.

Figure 6. Cycling runs for the photodegradation of RhB by the ZnO-NRs/TPNiPc hierarchical hetero-nanostructure arrays assisted with H_2O_2 under visible light irradiation.

Figure 7. (a) UV–vis diffuse reflectance spectra of the as-prepared ZnO–NRs/TPNiPc hierarchical hetero-nanostructures, TPNiPc and ZnO–NRs at room temperature. (b) Plots of the $(\alpha h\nu)^2$ vs. photon energy ($h\nu$) for the as-obtained samples.

Figure 8. (a) *I–V* curves of ZnO–NRs/TPNiPc hierarchical hetero-nanostructure arrays measured in dark and under illumination by using a 300 W Xe lamp (15A), respectively; (b) Photocurrents of the ZnO–NRs/TPNiPc hierarchical hetero-nanostructure arrays under the visible light of different power.

Figure 9. *I–V* curves of ZnO–NRs/TPNiPc hierarchical hetero-nanostructure arrays assisted with H_2O_2 measured in dark and under illumination by using a 300 W Xe

lamp (15A), respectively.

Scheme 1. Schematic illustration of the fabrication of the ZnO–NRs/TPNiPc hierarchical heteronanostructures: (a) zinc foil was inserted into the first solution; (b) needle-like ZnO–NRs grew on both sides of zinc foil; (c) ZnO–NRs covered on zinc foil was inserted into the second solution; (d) TPNiPc hierarchical hetero-nanostructure assembled onto the top of needle -like ZnO–NRs.

Scheme 2. Illustrative diagram for the photocatalytic mechanism of ZnO–NRs/TPNiPc hierarchical hetero-nanostructure assisted with H_2O_2, VB = valence band, CB = conduction band, HOMO = highest occupied molecular orbital and LUMO = lowest occupied molecular orbital.

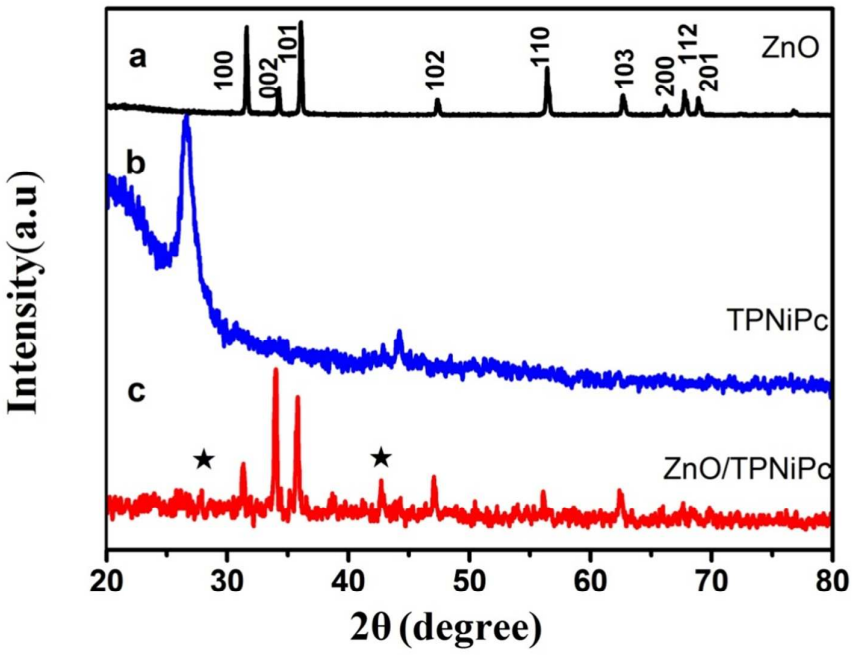

Figure 1. XRD patterns of ZnO–NRs/TPNiPc hierarchical hetero-nanostructures, TPNiPc and ZnO–NRs.

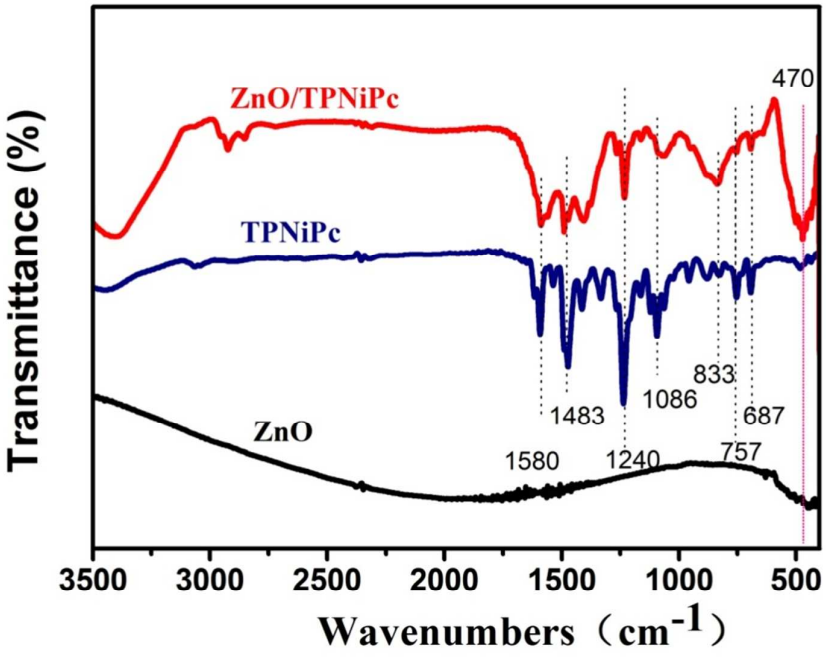

Figure 2. FTIR spectra of ZnO–NRs/TPNiPc hierarchical hetero-nanostructures, TPNiPc and ZnO–NRs.

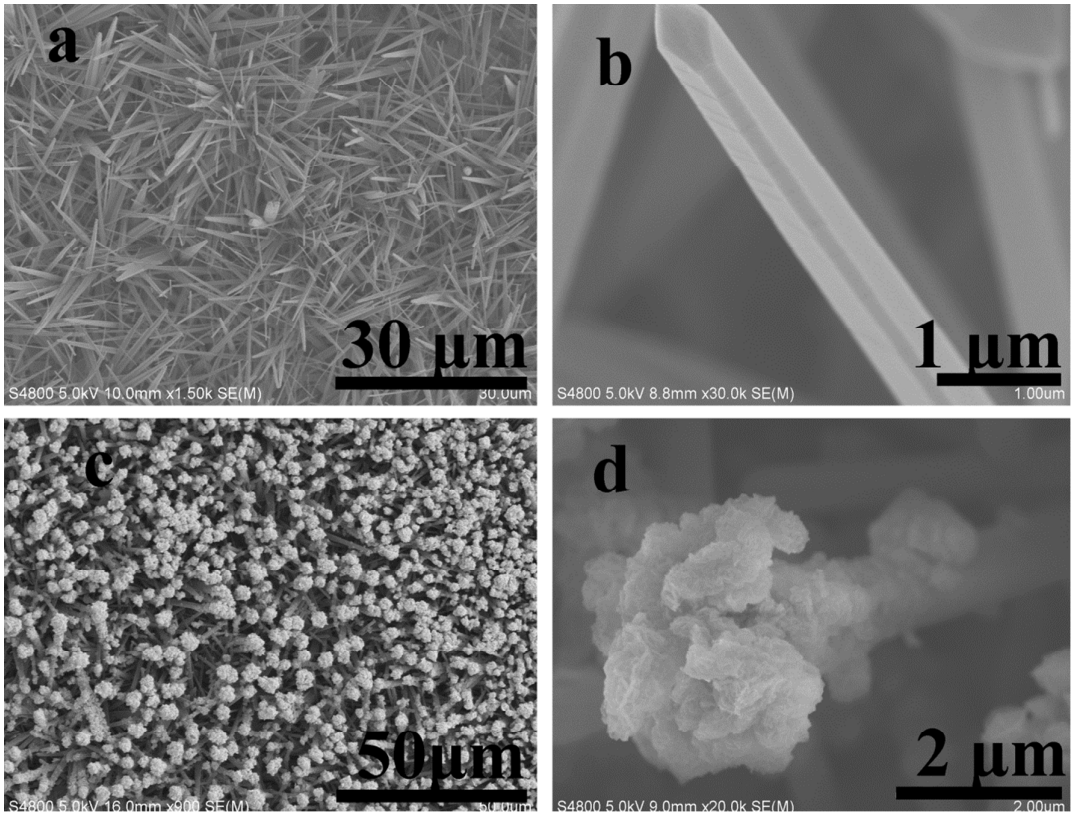

Figure 3. (a, b) FESEM images of ZnO–NRs; (c, d) FESEM images of the ZnO–NRs/TPNiPc hierarchical hetero-nanostructures.

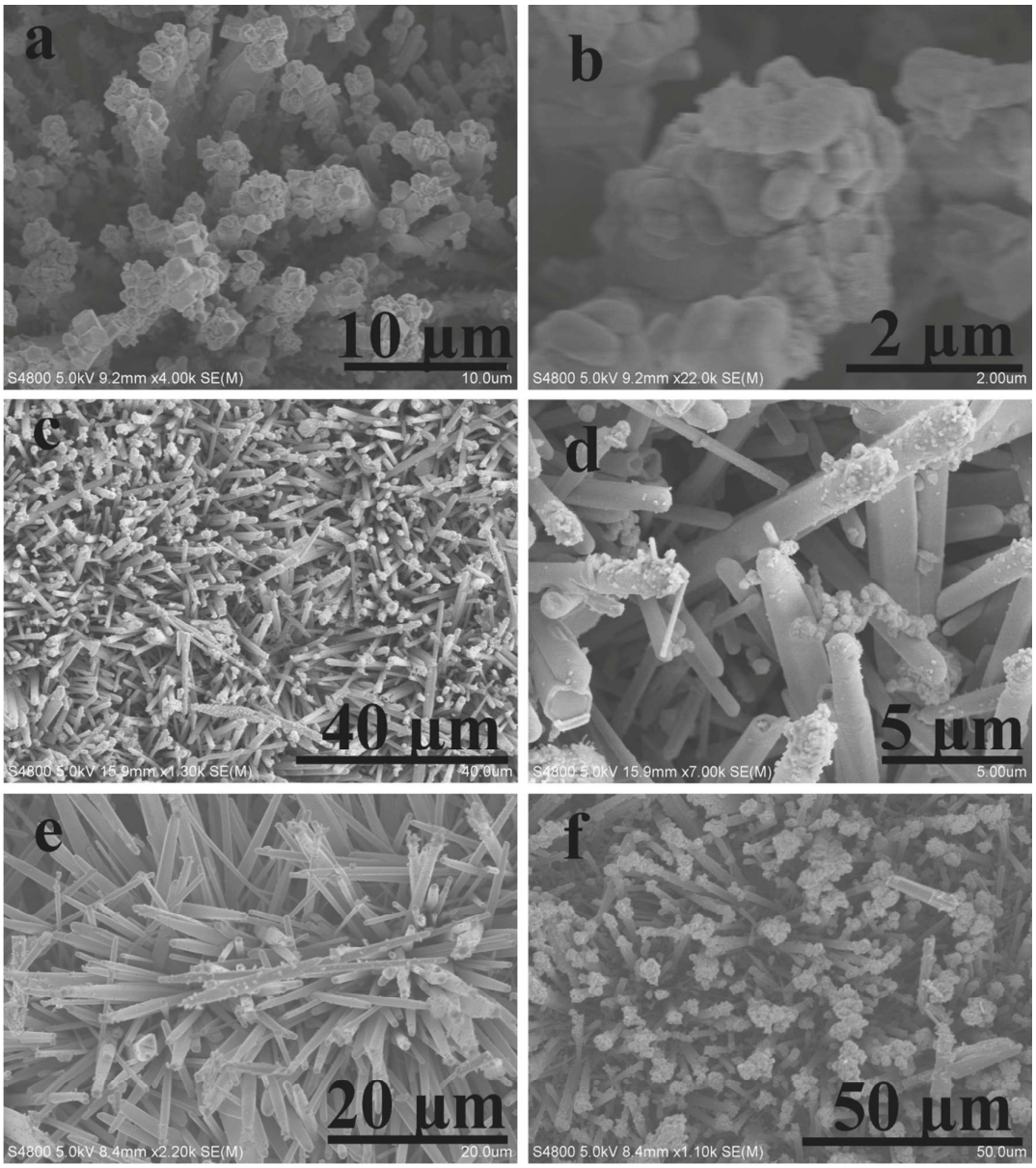

Figure 4. FESEM images of the ZnO–NRs/TPNiPc hierarchical hetero-structures attained at different reaction conditions: (a, b) at 200 ^{o}C; (c, d) the dosage of 4-Phenoxyphthalonitrile is 0.025 g; (e) the heating time is under 5 h; (f) the heating time is about 10 h.

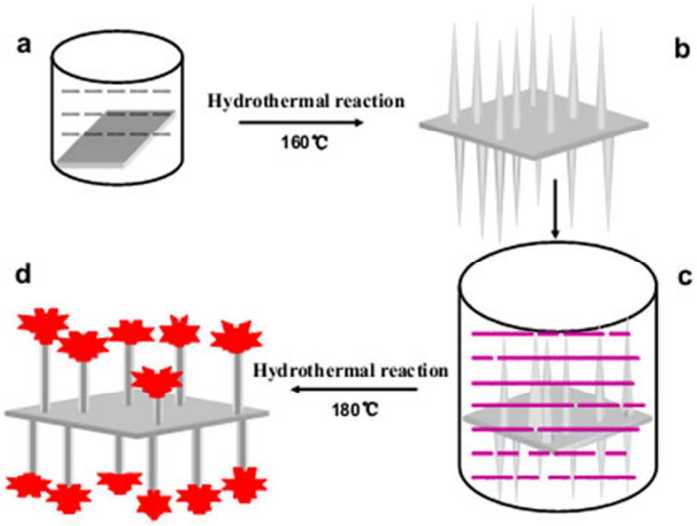

Scheme 1. Schematic illustration of the fabrication of the ZnO–NRs/TPNiPc hierarchical heteronanostructures: (a) zinc foil was inserted into the first solution; (b) needle-like ZnO–NRs grew on both sides of zinc foil; (c) ZnO–NRs covered on zinc foil was inserted into the second solution; (d) TPNiPc hierarchical hetero-nanostructure assembled onto the top of needle -like ZnO–NRs.

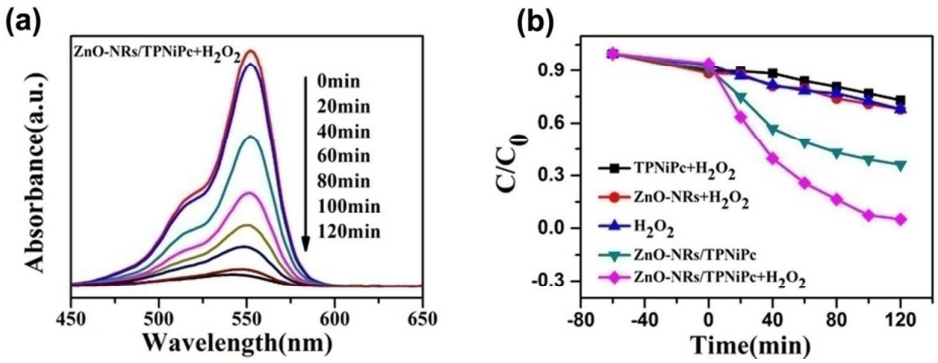

Figure 5. (a) Absorption spectra of the RhB solution by ZnO–NRs/TPNiPc hierarchical hetero-nanostructures assisted with H_2O_2 under visible light irradiation; (b) RhB photodegradation curves of C/C_0 versus time by ZnO–NRs/TPNiPc hierarchical hetero-nanostructures assisted with or without H_2O_2, TPNiPc assisted with H_2O_2, ZnO–NRs assisted with H_2O_2 and pure H_2O_2 under visible light irradiation, where C_0 and C are the initial concentration and the reaction concentration of RhB, respectively.

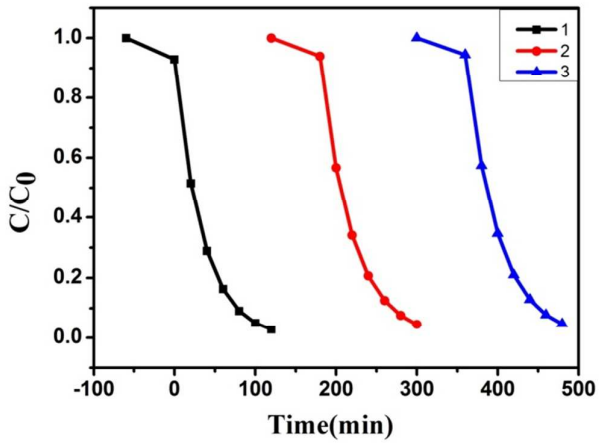

Figure 6. Cycling runs for the photodegradation of RhB by the ZnO-NRs/TPNiPc hierarchical hetero-nanostructure arrays assisted with H_2O_2 under visible light irradiation.

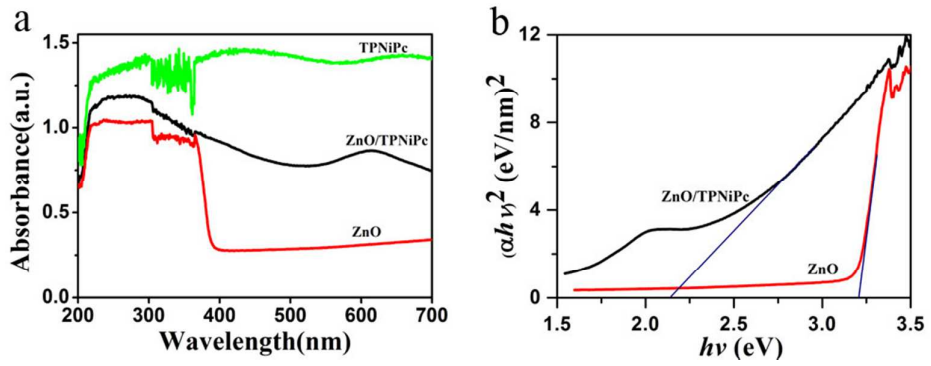

Figure 7. (a) UV–vis diffuse reflectance spectra of the as-prepared ZnO–NRs/TPNiPc hierarchical hetero-nanostructures, TPNiPc and ZnO–NRs at room temperature. (b) Plots of the $(\alpha h\nu)^2$ vs. vs. photon energy ($h\nu$) for the as-obtained samples.

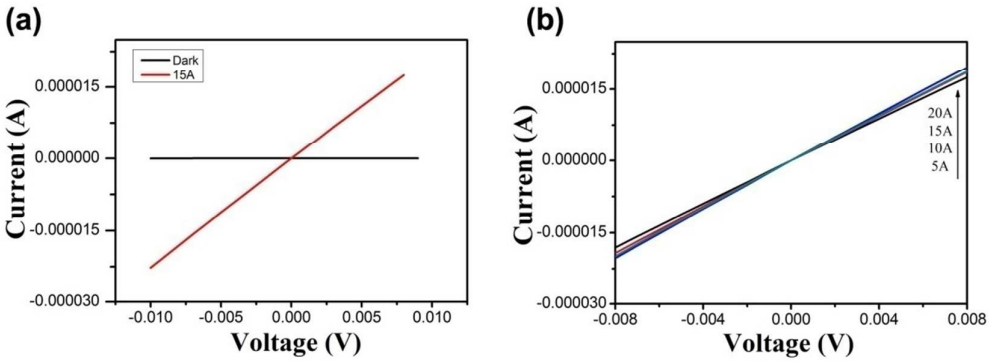

Figure 8. (a) *I–V* curves of ZnO–NRs/TPNiPc hierarchical hetero-nanostructure arrays measured in dark and under illumination by using a 300 W Xe lamp (15A), respectively; (b) Photocurrents of the ZnO–NRs/TPNiPc hierarchical hetero-nanostructure arrays under the visible light of different power.

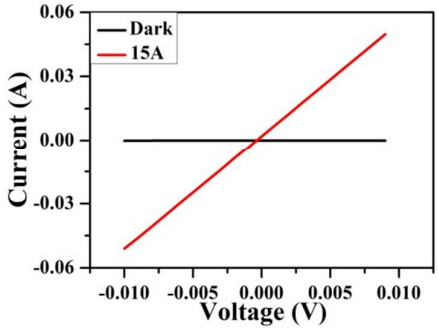

Figure 9. *I–V* curves of ZnO–NRs/TPNiPc hierarchical hetero-nanostructure arrays assisted with H_2O_2 measured in dark and under illumination by using a 300 W Xe lamp (15A), respectively.

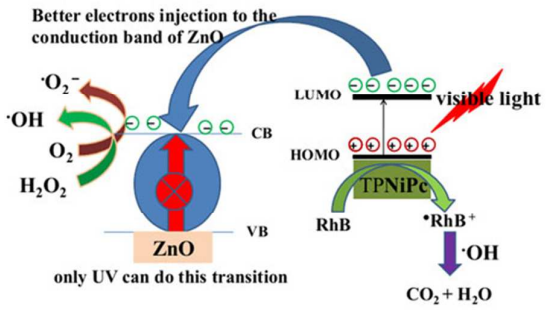

Scheme 2. Illustrative diagram for the photocatalytic mechanism of ZnO–NRs/TPNiPc hierarchical hetero-nanostructure assisted with H_2O_2, VB = valence band, CB = conduction band, HOMO = highest occupied molecular orbital and LUMO = lowest occupied molecular orbital.